A novel joint space-wavenumber analysis of an unusual Antarctic gravity wave event

R. G. Stockwell,[1] M. J. Taylor,[2,3] K. Nielsen,[2,3] and M. J. Jarvis[4]

[1] As part of a collaborative research program between British Antarctic Survey, U.K. and Utah State University, USA, all sky airglow images were recorded at Halley Station Antarctica (75.5 S, 26.7 W). An unusual mesospheric gravity wave event was observed in the OH nightglow (nominal height ≈87 km) over a period of ≈3 hours on the 27–28 May, 2001. The characteristics of the bore wave event were determined by application of the one dimensional spatial S-Transform analysis. This is the first time such analysis has been performed on airglow data. By employing these local spatial spectral analysis, the evolution of the wave packet can be measured. The wave parameters (phase velocity, wave number, wavelength, period) were inferred from as little as 2 images (separated in time), which is a powerful ability when a data set of images is irregularly sampled in time, as is often the case in airglow imager studies. Several interesting and novel results were obtained regarding the dynamic evolution of the wave. The horizontal wavelength of the bore wave packet was seen to decrease as the packet evolved. Coincident with this observation, the horizontal phase speed decreased, with an associated decrease in wave packet amplitude. **Citation:** Stockwell, R. G., M. J. Taylor, K. Nielsen, and M. J. Jarvis (2006), A novel joint space-wavenumber analysis of an unusual Antarctic gravity wave event, *Geophys. Res. Lett.*, *33*, L08805, doi:10.1029/2005GL025660.

1. Introduction

[2] Mesospheric bores [*Dewan and Picard*, 1998] are rare wave events that have previously only been reported at low and mid latitudes. The first reported observation of a bore event was by *Taylor et al.* [1995], a sharp front was observed in the airglow propagating horizontally, followed by a large amplitude wave train. The wave train was seen to have a horizontal wavelength of 20 km, and a horizontal phase speed of 75 m/s. Since then, several bore-like events have been observed in mid latitudes [*Smith et al.*, 2003; *She et al.*, 2004; *Brown et al.*, 2004] and low latitudes [*Smith et al.*, 2005; *Medeiros et al.*, 2005]. Further studies of mesospheric bore observations have linked the occurrence of bores to thermal inversion layers [*She et al.*, 2004]. Mesospheric bores have been seen to propagate over distances as great as 1200 km [*Smith et al.*, 2003].

---
[1]Colorado Research Associates Division, Northwest Research Associates Inc., Boulder, Colorado, USA.
[2]Center for Atmospheric and Space Sciences, Utah State University, Logan, Utah, USA.
[3]Department of Physics, Utah State University, Logan, Utah, USA.
[4]British Antarctic Survey, Cambridge, UK.

[3] All-sky CCD observations in the OH, Na, and O_2 emissions have been made from Halley Station Antarctica (75.5 S, 26.7 W) as part of a collaborative research program between British Antarctic Survey, U.K. and Utah State University, USA. The bore event was observed over a period of several hours on 27 May, 2001. A one dimensional local spectral analysis is employed to determine the wave characteristics using the well sampled OH data. A similar local temporal spectral analysis was successfully used to estimate the characteristics of quasi-monochromatic gravity waves observed with a scanning radiometer [*Stockwell and Lowe*, 2001b, 2001a]). In this application however, the local nature of the analysis is exploited to probe the temporal evolution of the bore wave packet.

2. Data Processing

[4] The data consists of a series of OH all sky images recorded every 2 minutes (with occasional calibration breaks) on May 27, 2001. The spatial sampling interval of the images is 586m. Flat field corrections were applied to the image series. Each image of the data set was spatially (x, y) bandpass filtered with a second order butterworth filter with a low wave number cut-off at 0.016 km^{-1} (corresponding to a 62.5 km wavelength) and a high wave number cut-off at 0.5 km^{-1} (corresponding to a 2 km wavelength). The slowly moving milky way and star signals were removed with application of a temporal high pass filter applied in the time domain to each pixel's time series with a lower cutoff frequency of 0.00125 Hz (corresponding to a 13.3 min period). Temporal gaps in the data were linearly interpolated before application of the filter, and these interpolated points were discarded after the filtering operation.

3. Bore Wave Packet

[5] A large amplitude wave event (mesospheric bore) is clearly evident propagating from the top edge of the field of view in Figure 1. The wave packet extends along the phase front across the entire field of view, greater than 500 km. Perpendicular to the wave front, the packet is approximately 200 to 300 km long, with many wave crests and troughs visible. The direction of propagation is due south. Accompanying the wave packet is a significant step increase in OH brightness propagating southward at the same speed as the wave crests (especially evident in the 18:38 UT image, where the bottom left of the image is much darker than the wave trough in the upper half of the image). Because of i) the step function nature of the bore wave packet, ii) the phase locked wave fronts moving with the step function, and iii) the increased number of trailing
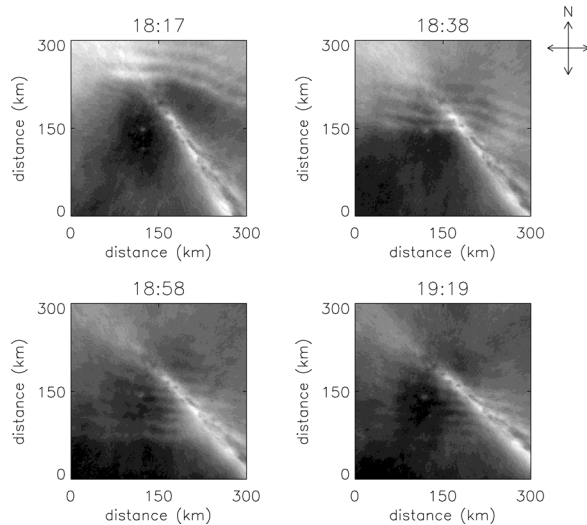
Figure 1. OH intensity measured at Halley Bay, Antarctica on May 27, 2001. A strong wave packet is seen travelling southward. The bright diagonal feature is the Milky Way.

wave crests forming within the imagers field of view [*Nielsen et al.*, 2006], it is concluded that this event is a bore phenomenon [*Dewan and Picard*, 1998, 2001]. Nielsen observed that 6.6 waves per hour were being generated during this bore event, which is higher (2.8 waves per hour) than would be expected by Dewan and Picard's theory.

4. One Dimensional Spatial Local Spectral Analysis

[6] One dimensional spatial S-Transforms were performed along the direction of wave propagation (along the y direction) for a specific image (t_0) and a specific column (x_0).

$$data(x_0, y, t_0) \rightarrow_{y \rightarrow k_y} S(x_0, y, ky, t_0) \quad (1)$$

[7] The local temporal spectrum was not analyzed because of the irregular sampling in time. A sampling interval of 2 minutes between frames gives a Nyquist Frequency (highest resolvable frequency) corresponding to a period of 4 minutes. The peak period of the wave event is close to this lower limit. If a wave is not sampled quickly enough in time, the signal is aliased, and will appear at a lower and incorrect frequency region.

[8] Indeed, during the infrequent calibration gaps, the recorded time series is aliased. Because of this aliasing of the wave in time, it is difficult to correctly characterize the wave using temporal Fourier, or temporal local spectral methods. However, the wave is well sampled in the spatial domain due to the very high spatial resolution of the imager. In fact, one can compare spatial phase shifts of the wave between successive images (sampled every 2 minutes) and thus fully characterize this wave by measuring horizontal wave number and horizontal phase velocity. With this information and application of linear gravity wave theory, one can infer the temporal frequency. The advantage of this approach is that it does not require uniform sampling in

time, as any two images (taken ≈2 minutes apart) are more than adequate to calculate the phase progression between local spatial spectra of each image.

[9] In order to isolate strong quasi-monochromatic wave events, the amplitude of the local spatial S-Transform peaks were compared to a threshold amplitude (equal to 60 brightness units). This threshold was based on a statistical analysis of a dark region of the image (i.e., no wave signature). The S-Transform of this region was calculated and the amplitudes were determined. Calculations on these dark region results indicated that an S-Transform amplitude of 50 units was at the 99.94% confidence level (i.e., 99.94% of the ST amplitudes of the dark region fell below the threshold of 50 units). A threshold of 60 units was chosen to be higher than any of the dark S-Transform amplitudes. Based on this analysis, the chance of random fluctuations exceeding this threshold is vanishingly small (less than 0.01 percent). A large peak in S-Transform amplitude was seen at ≈25 km wavelength which corresponds to the bore wave packet. The position of this peak indicates the peak wave number of the wave packet. In this preprocessed and filtered data set, the bore wave packet was by far the dominant feature in the local amplitude spectrum, allowing us to track the peak spectral amplitude even as it changed its position (i.e., as the peak wave number of the bore wave packet increased as time progressed).

[10] The phase can be directly read from the S-Transform [*Stockwell et al.*, 1996]. By employing a cross S-Transform analysis the phase ϕ of the cross S-Transform function at the peak wave number k_y is equal to the phase difference of the bore wave packet between the two images. Since the wavelength is known from the wave number, the distance traveled can be calculated. With knowledge of the distance the phase front traveled and also the time interval ($t_1 - t_0$) between the two images, the (observed horizontal) phase velocity of the wave packet can be calculated. This analysis is repeated for each pair of images throughout the night to infer the temporal evolution of the wave properties of the bore event.

5. Observed Wave Parameters

[11] The order of presentation of the bore wave characteristics follows that which is most readily available from the S-Transform analysis. A numerical simulation of these calculations shows an error in the estimated phase of 0.01 radians, which lead to a 1.4% estimated error in the wave parameters.
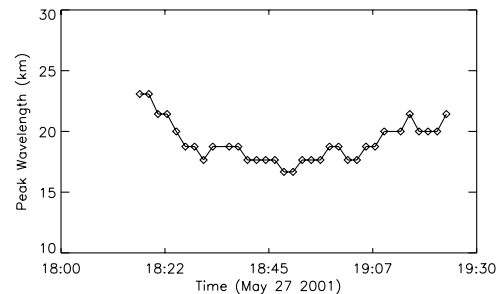

Figure 2. Peak S-Transform horizontal wavelength (km) of the wave as a function of time.
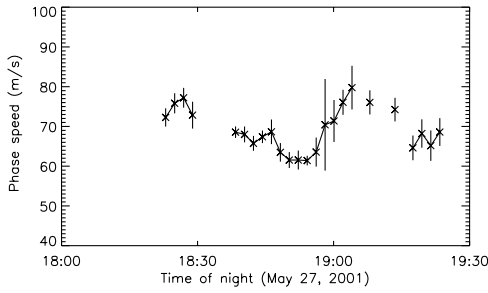
Figure 3. Inferred observed phase speed (m/s) of the wave as a function of time.

5.1. Horizontal Wavelength

[12] The horizontal wave number (k_y) and thus horizontal wavelength of a quasi-monochromatic wave can be read directly from the peak amplitude of the S-Transform. This is shown in Figure 2 where the wavelength of the bore wave packet is plotted as a function of time of night. The wave packet initially has a wavelength of ≈25 km and decreases to ≈18 km. Data is plotted only where the S-Transform amplitude is above the threshold value. The decrease in wavelength takes place from approximately 18:15 UT to 18:30 UT.

5.2. Observed Horizontal Phase Speed

[13] Cross spectral S-Transform analysis can be used to calculate the spatial phase difference. The Cross S-Transform Function ($C[y, k_y]$) is defined as

$$CrossST\left[x_0, y, k_y, t_0\right] = S_1\left[x_0, y, k_y, t_0\right] * S_2\left[x_0, y, k_y, t_1\right]* \quad (2)$$

where the * indicates complex conjugate and S_1 and S_2 are the spatial S-Transforms of two space domain series (i.e., a column of the image). Here, $S_1[x_0, y, k_y, t_0]$ and $S_2[x_0, y, k_y, t_1]$ are of the same column (i.e., x_0) from successive images taken at a time difference of $\Delta t = t_1 - t_0$. The phase of $C[x_0, y, k_y, t_0]$ indicates the phase shift ϕ between the two space domain series over a time $\Delta t = t_1 - t_0$. The distance a phase front travels between images is calculated by

$$\Delta D = \lambda \frac{\phi}{2\pi} \quad (3)$$

Knowing the wavelength λ of this wave, one can infer the phase speed as

$$V_{ph} = \frac{\phi}{2\pi} * \frac{\lambda}{\Delta t} \quad (4)$$

Note: here Δt is NOT equal to the period of the wave, it is the time sampling interval between images, hence the preceding phase term. One only needs 2 images to measure a horizontal wave number phase shift. As long as the wave number of the wave is well sampled (the horizontal resolution of these images allows one to measure wavelength down to roughly one km) and the phase speed of the wave is such (i.e., low enough) that the phase shift between two images is less than one half of a wavelength, then the speed can be resolved. The phase of the wave in each image is necessarily restricted to the range of $-\pi$ to π. Thus the maximum phase difference must be less than π radians (or else one could add an arbitrary multiple of 2π so that the difference was less than π). Hence the maximum measurable phase speed is

$$V_{ph}MAX = \frac{\pi}{2\pi} * \frac{\lambda}{\Delta t} \quad (5)$$

and hence the maximum frequency that can be inferred from this method is

$$f_{\max} = \frac{V_{phMAX}}{\lambda} = \frac{\pi}{2\pi} * \frac{1}{\Delta t} = \frac{1}{2\Delta t} \quad (6)$$

which gives us the Nyquist frequency.

[14] While only one image is required to measure a horizontal wavelength, as in Figure 2, two successive images are required in order to infer a phase velocity. If the time elapsed between the two images is too large, one cannot unambiguously measure the phase shift and therefore one cannot measure the phase velocity. Other inferred values such as wave period also suffer. Because of gaps due to calibration, there are some missing points in phase velocity and wave period.

[15] In Figure 3 the observed horizontal phase speed is plotted as a function of time. Values of phase speed are plotted only where the corresponding S-Transform amplitude peak is above the threshold. The phase speed has a consistent value in the range from 70 m/s to 80 m/s.

5.3. Observed Period

[16] Calculation of the (observed) phase speed of the wave allows one to infer the (observed) frequency and period of the wave, where the period is equal to

$$T = \frac{1}{f} = \frac{\lambda}{V_{ph}} \quad (7)$$

The observed period of the bore wave front is shown in Figure 4. During the largest deceleration of the wave (18:15 to 18:30) the period of the wave is relatively stable at a value of approximately 5 minutes, while the wavelength undergoes its largest change, from 25 to 18 km.

5.4. Wave Packet Motion

[17] Since the S-Transform amplitude can localize the wave energy in space for a quasi-monochromatic wave, the peak amplitude can be tracked over time to measure the
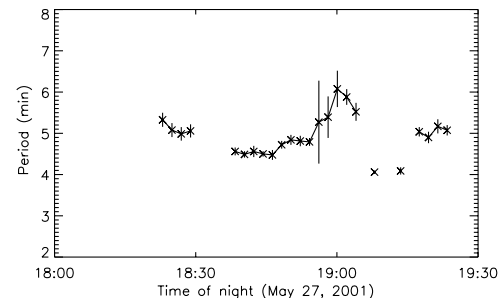

Figure 4. Inferred observed period (minute) of the bore wave packet as a function of time of night.
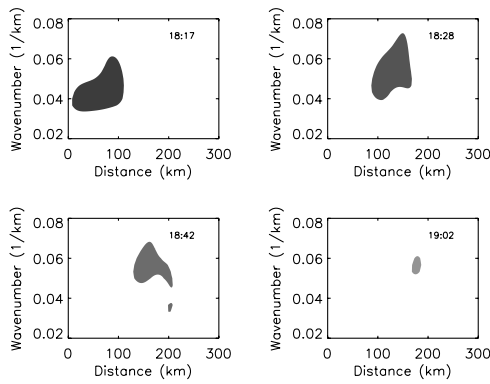
Figure 5. Contours of the spatial S-Transform amplitudes (wave number vs southward distance) at four different times. As the wave packet evolves, the horizontal wave number increases. Also, the wave packet can be seen to move into the field of view (distance = 0 km) but the amplitude dies out and it does not leave the field of view (distance = 300 km).

position of the wave group as a function of time over the night. The position of the group of the wave can be seen in Figure 5, where S-Transform amplitudes ($S(x_0, y, k_y, t_i)$ for many images "i") from many successive images are overplotted. Values below 60 units are not shown. The motion of the wave packet is apparent from the contour plots. The wave packet is centered at about 60 km at 18:17 UT, 110 km at 18:28 UT, 150 km at 18:42 UT, and at 180 km at 19:02. The amplitude of the wave packet is also changing over this time period, and is all but attenuated at 19:02 UT.

[18] If one takes the peak amplitude position of the S-Transform ($S(x_0, y, k_y, t_i)$) once can measure the changing position of the wave packet as shown in Figure 6.

[19] The observed horizontal group velocity of the packet slows dramatically, at roughly 18:30 UT. The S-Transform amplitude can be tracked for this wave over time to measure the changing amplitude over the night, as shown in Figure 7. Coincident with the deceleration of the horizontal group speed is the decrease in the bore wave packet's amplitude.

[20] Because the analysis employed was one dimensional, it was not able to reveal some types of motions such a rotation of wave fronts. Visual inspection of the raw data images indicates that the wave did propagate to the south direction, and that no significant wave front rotation occurred. Some of the parameters reported here (speeds and
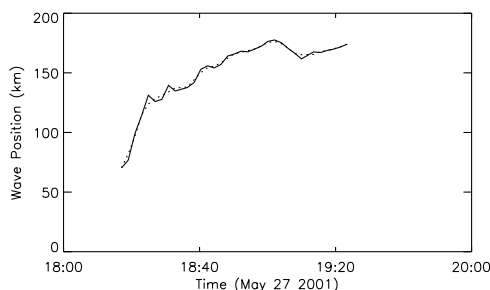

Figure 6. Peak S-Transform position (southward distance) of the wave group as a function of time.
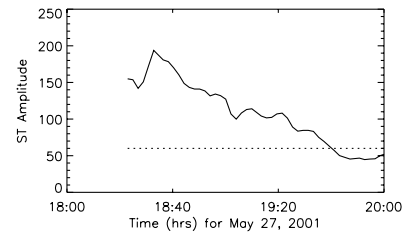

Figure 7. Spatial S-Transform amplitude of the wave group as a function of time. The horizontal dashed line indicates the statistical threshold level of 60 units.

frequency) are "observed" parameters, and hence knowledge of the background winds is required to infer "intrinsic" values before comparing the results with other measurements. This analysis has been carried out by *Nielsen et al.* [2006] using coincident wind measurements from the BAS Imaging Doppler Interferometer (IDI). At 18:15 UT, the wave packet is traveling in the direction of the background wind thus the intrinsic phase speed is higher than the observed phase speed by approximately 35 m/s. By 19:00 UT the background wind speed has been reduced to nearly zero, and thus the intrinsic and the observed phase speeds are the same.

[21] A full two (spatial) dimensional S-Transform analysis will be pursued in a future project. This is described in more detail in R. Stockwell et al. (Two dimensional S-Transform analysis of the evolution of a mesospheric bore wave packet, manuscript in preparation, 2006).

6. Summary

[22] An unusual mesospheric bore event was observed in the OH nightglow (≈87 km) over a period of ≈3 hours on the 27–28 May, 2001. This wave packet was identified as a bore event due to the presence of a step function increase of the OH brightness that propagates locked to the phase speed of the trailing wave packet. The characteristics of the bore wave event were determined by application of the one dimensional spatial S-Transform analysis. Such parameters (phase velocity, group velocity, wavelength, period) were inferred from as little as 2 images (separated in time), which is a powerful ability when a data set of images is irregularly sampled in time, as is often the case in airglow imager studies. The horizontal wavelength of the bore wave packet decrease as the packet evolved. Coincident with this observation, the horizontal phase speed decreased, with an associated decrease in wave packet amplitude.

References

Brown, L. B., A. J. Gerrard, J. W. Meriwether, and J. J. Makela (2004), All-sky imaging observations of mesospheric fronts in OI 557.7 nm and broadband OH airglow emissions: Analysis of frontal structure, atmospheric background conditions, and potential sourcing mechanisms, *J. Geophys. Res.*, *109*, D19104, doi:10.1029/2003JD004223.

Dewan, E., and R. Picard (1998), Mesospheric bores, *J. Geophys. Res.*, *103*, 6295–6305.

Dewan, E., and R. Picard (2001), On the origin of mesospheric bores, *J. Geophys. Res.*, *106*, 2921–2927.

Medeiros, A., J. Fechine, R. Buriti, H. Takahashi, C. Wrasse, and D. Gobbi (2005), Response of OH, O2 and OI5577 airglow emissions to the meso-

spheric bore in the equatorial region of brazil, *Adv. Space Res.*, *35*, 1971–1975.

Nielsen, K., M. J. Taylor, R. G. Stockwell, and M. J. Jarvis (2006), An unusual mesospheric bore event observed at high latitudes over Antarctica, *Geophys. Res. Lett.*, *33*, L07803, doi:10.1029/2005GL025649.

She, C. Y., T. Li, B. P. Williams, T. Yuan, and R. H. Picard (2004), Concurrent OH imager and sodium temperature/wind lidar observation of a mesopause region undular bore event over Fort Collins/Platteville, Colorado, *J. Geophys. Res.*, *109*, D22107, doi:10.1029/2004JD004742.

Smith, S. M., M. J. Taylor, G. R. Swenson, C. She, W. Hocking, J. Baumgardner, and M. Mendillo (2003), A multidiagnostic investigation of the mesospheric bore phenomenon, *J. Geophys. Res.*, *108*(A2), 1083, doi:10.1029/2002JA009500.

Smith, S., J. Friedman, S. Raizada, C. Tepley, J. Baumgardner, and M. Mendillo (2005), Evidence of mesospheric bore formation from a breaking gravity wave event: Simultaneous imaging and lidar measurements, *J. Atmos. Sol. Terr. Phys.*, *67*, 345–356.

Stockwell, R. G., and R. P. Lowe (2001a), Airglow imaging of gravity waves, 2, Critical layer filtering, *J. Geophys. Res.*, *106*, 17,205–17,220.

Stockwell, R. G., and R. P. Lowe (2001b), Airglow imaging of gravity waves, 1, Results from a small network of OH nightglow scanning imagers, *J. Geophys. Res.*, *106*, 17,185–17,204.

Stockwell, R., L. Mansinha, and R. Lowe (1996), Localization of the Complex Spectrum: The S Transform, *IEEE Trans. Signal Process.*, *44*, 998–1001.

Taylor, M. J., D. N. Turnbull, and R. P. Lowe (1995), Spectrometric and imaging measurements of a spectacular gravity wave event observed during the ALOHA-93 campaign, *Geophys. Res. Lett.*, *22*, 2849–2852.

—————————

M. J. Jarvis, British Antarctic Survey, High Cross, Madingley Road, Cambridge CB3 0ET, UK.

K. Nielsen and M. J. Taylor, Center for Atmospheric and Space Sciences, Utah State University, Logan, UT 84322–4145, USA.

R. G. Stockwell, Colorado Research Associates Division, Northwest Research Associates Inc., 3380 Mitchell Lane, Boulder, CO 80301, USA. (stockwell@co-ra.com)